Accepted Manuscript

Strength enhancement of aluminium honeycombs caused by entrapped air under dynamic out-of-plane compression

S. Xu, J.H. Beynon, D. Ruan, T.X. Yu

PII: S0734-743X(12)00042-5

DOI: 10.1016/j.ijimpeng.2012.02.008

Reference: IE 2083

To appear in: *International Journal of Impact Engineering*

Received Date: 11 October 2011

Revised Date: 16 February 2012

Accepted Date: 19 February 2012

Please cite this article as: Xu S, Beynon JH, Ruan D, Yu TX, Strength enhancement of aluminium honeycombs caused by entrapped air under dynamic out-of-plane compression, *International Journal of Impact Engineering* (2012), doi: 10.1016/j.ijimpeng.2012.02.008

Strength Enhancement of Aluminium Honeycombs Caused by Entrapped Air under Dynamic out-of-plane Compression

S. Xu[1,2,*], J. H. Beynon[1], D. Ruan[1] and T. X. Yu[3]

[1]Faculty of Engineering and Industrial Sciences,
Swinburne University of Technology, Hawthorn, VIC 3122, Australia
[2]School of Mechanical and Power Engineering,
East China University of Science and Technology, Shanghai 200237, P. R. China
[3]Department of Mechanical Engineering,
Hong Kong University of Science and Technology, Clear Water Bay, Hong Kong

Abstract

The out-of-plane crushing behaviour of aluminium hexagonal honeycombs containing different percentages of holes (i.e., the fraction of penetrated cells to the total) was extensively investigated over a wide range of strain rates where each test was conducted at constant compression velocity. Strength enhancement due to the increase of the strain rate and the entrapped air was studied. It is found that the strain hardening of honeycomb structures during the dynamic crush is mostly attributed to the pressure change caused by the entrapped air. The leaking rate, $\dot{\delta}$, was then studied and found to be dependent on the strain and strain rate, and independent of the wall thickness to edge length ratio, *t*/*l*. An empirical constitutive relation describing the plastic collapse stress in relation to the *t*/*l* ratio, the strain and strain rate is proposed, which agrees well with the experimental results.

Keywords: aluminium hexagonal honeycombs, out-of-plane compression, strain rate effect, entrapped air, constitutive relation

1. Introduction

* Corresponding author. Tel.:+61 3 9214 8258, Fax: +61 3 9214 8264, Email: sxu@swin.edu.au

Cellular solids, including foams and honeycombs, are widely used as energy absorbers and protective components in automotive, aerospace and other engineering sectors because of their high energy absorption capacity and high strength-to-weight ratio. Due to the increasing demands in safety and energy saving of vehicles, research on the mechanical properties of metallic foams and honeycombs has become more and more attractive in the past decades [1, 2]. Since the impact of vehicles is of great interest, e.g. the structural response in a car crash, numerous studies have been conducted focusing on the dynamic behaviour of these materials and structures, especially on their strain rate sensitivity.

It has been found that some closed-cell foams exhibit strain rate sensitivity [3-7], while open-cell foams do not [7-9]. The studies on the dynamic out-of-plane compression of honeycombs also showed strain rate sensitivity [10-15]. Due to the complexity of cellular materials, the causes of this macroscopic strain rate sensitivity are still in debate. In summary, the strength enhancement under high strain rate compression may come from four sources; i.e., strain rate sensitivity of cell wall material, micro-inertia effect, entrapped air and shock wave (for high velocity impact only). The rise of the internal pressure caused by the entrapped air during the dynamic compression is believed to be one of the main reasons to the strength enhancement by some researchers [1, 15]. Gibson and Ashby [1] proposed a method to evaluate the strength enhancement due to the air pressure increase for foam materials. However, few experimental studies on this issue have been conducted so far. Zhang and Yu [16] studied pressurized thin-walled circular tubes under axial crushing and found that the strength enhancement resulted from a direct effect of the air pressure increase and an indirect effect caused by the interaction between air pressure and tube wall buckling. Dawson et. al. [17] developed a comprehensive boundary value model for the contribution of viscous Newtonian fluid flow to the stress-strain response of a fluid-filled, elastomeric open cell foam under dynamic compression and verified it with experiments on low-density polyurethane foams.

In a parallel study of the out-of-plane dynamic behaviour of hexagonal honeycombs by Xu et al. [13], a strong strength enhancement was observed when the compressive velocity increased from 5×10^{-5} to 10 m/s, especially when the deformation occurred in the region close to the densification strain. The present paper will focus on the effect of entrapped air aiming at a better interpretation of the relationship between the entrapped air and the strength enhancement. In the present paper, honeycomb specimens were sandwiched between two thin fibre reinforced sheets, one of which contained a certain amount of holes. First, the leakage of the entrapped air was studied by using specimens with different percentages of holes in one of the thin sheets. Then, the strain rate sensitivity was studied via a series of compression tests under crushing velocities ranging from 5×10^{-5} to 5 m/s. Finally, a constitutive relation is proposed which reflects the relation between the dynamic plateau stress and the relative density, strain and strain rate.

2. Experiments

2.1 Materials and specimens

The honeycomb materials used in this work were commercial HexWeb® CR III corrosion specification aluminium honeycombs. The cell wall material was aluminium alloy 5052 with a H39 temper. Four types of honeycombs were tested and their properties are listed in Table 1, as supplied by the manufacturer.

In a parallel study [13], it was experimentally demonstrated that honeycomb specimens with 9×9 cells are sufficient to represent a large block of honeycomb. Therefore, using the same method, honeycomb specimens were carefully cut by sharp, thin knives to contain 9×9 cells for honeycombs 3.1-3/16-5052-.001N, 4.5-3/8-5052-.001 and 8.1-1/8-5052-.002N 3N. Honeycomb, 4.2-3/8-5052-.003N, had large cell size. The loading platen of the testing machine could only accommodate 5×5

cells for this honeycomb. Thus, specimens containing 5×5 cells were used for this type of honeycomb only.

In order to study the effect of the entrapped air on the honeycomb properties during dynamic crushing, every specimen was sealed by a layer of GMS Composites EP-280 films, whose properties are listed in Table 2, on each end. Honeycomb specimens covered by EP-280 films were sandwiched between two aluminium sheets (splints), and then kept in a heating furnace at 150 ^{o}C for 20 minutes with a weight standing on the aluminium sheet to achieve a good bonding and seal (Fig. 1a). The difference of the stress-strain curves for specimens with and without the heating treatment was experimentally investigated and it was proved that the effect of such heat treatment (150 ^{o}C for 20 minutes) was negligible. Thereafter, one layer of EP-280 film at one end of honeycomb specimen was penetrated by a sharp ended heated tool to obtain a certain number of holes. For simplification, in the following, η is defined as the *hole percentage*, i.e., the number of penetrated cells divided by the total number of cells (When honeycombs are compressed axially under standard testing conditions with or without film sealing at both ends or used as sandwich cores, those honeycombs with no holes (η=0%) are recommended). The 5×5 cells 4.2-3/8-5052-.003N specimen shown in Fig. 1b has a hole percentage of 52%. One layer of strong double sided glue was used to cover each end of the specimen (Fig. 1c). Then the glue covered on the EP-280 film with holes was penetrated again by the heated tool (Fig. 1d). Figure 1(e) shows a 9×9 cells 3.1-3/16-5052-.001N specimen with nominal 51% penetrated cells at one end. In the test, the end with holes was sitting on the support with many small holes (Fig. 2), from which the air could easily leak out of the specimen during a crushing test.

2.2 Equipment and test set-up

Quasi-static and low strain rate tests were conducted on an MTS machine. The MTS machine has a load capacity of 250 kN and can reach a velocity of up to 0.2 m/s for compression

tests. Specimens were sitting on the lower fixed platen. During the compression, the upper platen moved downwards to crush specimens. Velocities of 5×10^{-5}, 5×10^{-3} and 5×10^{-2} m/s, respectively, were applied to specimens corresponding to nominal strain rates of 10^{-3}, 10^{-1} and 1 s^{-1}, respectively, for specimens 50 mm thick.

Dynamic compression tests were conducted on an Instron 8800 hydraulic high rate testing system (Fig. 3). The Instron is equipped with VHS software, which helps to maintain a constant velocity during the compression of the specimens. The Instron can achieve a maximum velocity of 10 m/s in compression and has a load capacity of 100 kN. In our experiments, the Instron was used for tests under crushing velocities of 0.5 and 5 m/s, the corresponding nominal strain rates were 10 and 10^2 s^{-1}, respectively, for specimens 50 mm thick. A high speed camera was used to record the deformation process of honeycomb specimens in the dynamic out-of-plane compression.

In the parallel study [13], experimental data obtained from the MTS and Instron testing machines at a velocity of 5×10^{-2} m/s were in good agreement with each other. Therefore, the experimental data obtained from the two machines in the present study are comparable and can be analysed together. Moreover, reference [13] showed a good agreement for repeated tests, so that only one test was conducted for each test condition in the present study, unless otherwise stated.

The set-up of the present tests is sketched in Fig. 2. A specially designed support with holes was riveted to the lower load piston. The holes in the support had a diameter of 3.2 mm. While honeycomb specimens were placed on the support, the holes on one end of the specimen were against the holes in the support, which allowed the air in the specimens to escape easily.

2.3 Data processing

Periodical “Y” unit structures, which compose the cell structure around each triple point, were used to deal with the experimental data in the same way as that in the parallel study [13]. The relative density of perfect hexagonal honeycomb is related to the wall thickness to edge length ratio, t/l, for perfect hexagonal honeycombs ($h=l$, $\theta=30^o$) [1],

$$\frac{\rho^*}{\rho_s} = \frac{8}{3\sqrt{3}} t/l, \quad (1)$$

In calculating the nominal stress, the total area that "Y" units occupied was used. The stress was calculated by $\sigma=F/(N_Y S_Y)$, where F is the out-of-plane load, N_Y is the number of "Y" unit structures being contained in a specimen and S_Y is the area occupied by a single "Y" unit. Applying the energy efficiency method [18], the plateau stress, σ_{pl}^*, can then be calculated by

$$\sigma_{pl}^* = \frac{\int_0^{\varepsilon_d} \sigma(\varepsilon) d\varepsilon}{\varepsilon_d} \quad (2)$$

where ε_d represents the densification strain of the honeycomb during its out-of-plane compression. Table 3 summarizes all the tests conducted in the present study and the calculated densification strains and plateau stresses.

3. Experimental results and discussions

3.1. Strain rate sensitivity

Quasi-static and dynamic compression tests were conducted under various velocities ranging from 5×10^{-5} to 5 m/s. The stress-strain curves were plotted in Figs. 4 to 6 for honeycomb 3.1-3/16-5052-.001N (H31), 4.5-1/8-5052-.001N (H45) and 8.1-1/8-5052.002N (H81), respectively. It can be seen that with the increase of the compression velocity, the plateau stress increases accordingly. As shown in Table 4, for honeycomb specimens without holes, the plateau stress increased by 29.4%, 24.5% and 18.5% for H31, H45 and H81, respectively. For honeycomb specimens with 100% holes, the plateau stress increased by 21.1%, 22.3% and 16.1% for H31, H45 and H81, respectively. For specimens with 51% holes, the values are 30.0%, 25.0% and 19.3% for H31, H45 and H81, respectively. These results revealed that strain rate has great influence on the plateau stress, which is in agreement with the parallel study [13] and other researchers' findings [10-12, 14, 15]. In reference [13], the support was a solid flat platen without holes. Thus, the entrapped air had little

chance to leak from the specimens during compression. Therefore, the stress-strain curves obtained in [13] are similar to those from the specimens with 0% or 51% holes in the present study, although they were not sealed.

In quasi-static out-of-plane compression of honeycombs, the mean plateau stress (σ_{pl}^{*}) is related to the relative density, i.e. the wall thickness to edge length ratio (t/l), which can be expressed by

$$\sigma_{pl}^{*} = C_0 \sigma_{ys} (t/l)^{k_3} \tag{3}$$

where C_0 and k_3 are coefficients. By fitting the mean plateau stress values obtained from the quasi-static ($\dot{\varepsilon}$ =10^{-3} s^{-1}) compression of specimens containing different numbers of the holes into Eq. (3), C_0 and k_3 can be obtained, as listed in Table 5. Fitted curves are plotted in Fig. 7. For specimens with more holes, C_0 increases from 4.05 to 4.62 while k_3 increases from 1.51 to 1.55. Since t/l<<1, the increase of k_3 leads to a decrease of σ_{pl}^{*}, while the increase of C_0 results in an increase of σ_{pl}^{*}. With the increase of both C_0 and k_3, σ_{pl}^{*} may keep the same. As shown in Fig. 7, all three fitted curves are almost coincident. Therefore, the number of the holes in the specimens has little influence on the macroscopic properties of honeycombs in quasi-static compression.

The same method as that used in the parallel study [13] is employed to evaluate the relationship between plateau stress (σ_{pl}^{*}) and strain rate ($\dot{\varepsilon}$) under dynamic compression, which has a form of

$$\sigma_{pl}^{*} = C_1 \sigma_{ys} (t/l)^{k_3} (1 + C_2 \dot{\varepsilon})^{p} \tag{4}$$

where σ_{ys} is the yield stress of the cell wall material, and σ_{ys}=292 MPa in the present study. C_1, C_2, and p are coefficients to be determined from the tests. k_3 is determined from Eq. (3) and it is supposed to be unchanged during the dynamic compression. C_0 and C_1 in Eqs. (3) and (4) may not be exactly the same during the fitting since a strain rate term is introduced. By taking experimental

values of the mean plateau stress of each honeycomb specimen with t/l ratio of 0.00924, 0.0139 and 0.0277, respectively, C_1, C_2 and p are then fitted for honeycombs with different percentages of holes. The fitted curves are plotted in Fig. 8 and the values are listed in Table 5. It should be mentioned that C_2 would not change with specimen length since it has been experimentally demonstrated that specimen length has negligible effect on the plateau stress [13].

3.2 Strength enhancement caused by the entrapped air

Figures 4 to 6 also demonstrate the influence of the number of holes on the stress-strain curves. If all the cells of honeycomb specimens at one end were penetrated, i.e., η=100%, the stress-strain curves were flat (i.e. the stress did not increase with strain in the plateau region) for almost all the strain rates studied. While if there was no hole in the specimens, i.e., η=0%, the stress-strain curves had a comparatively flat shape for lower strain rate and the gradient increased at the end of the plateau region for higher strain rates. It can be seen from Figs. 4 to 6 that strength enhancement is evident only when the strain and strain rate are higher than certain values. The thresholds for strain (ε_{cr}) and strain rate are approximately 0.5 and 1 s^{-1} (i.e., crushing velocity v=0.05 m/s), respectively. Under high strain rate compression, when $\varepsilon > \varepsilon_{cr}$, a rise in the stress can be seen, especially for honeycomb with lower t/l ratio, e.g., 3.1-3/16-5052-.001N. In short, the increase of stress when $\varepsilon > \varepsilon_{cr}$ contributes a main part to the increase of the plateau stress in dynamic compression.

Although the source of strength enhancement in dynamic compression of cellular materials is a combination of multiple factors, the present study focuses on the effect of the entrapped air. Following Zhang and Yu's argument [16], ignoring the volume change due to the buckling and assuming the process is isothermal, the leakage of the air during the crushing can be defined by

$$\delta = 1 - \frac{PV}{P_0 V_0} \tag{5}$$

where P_0 and P are the initial pressure (atmospheric pressure) and the pressure when the displacement reaches a certain value, x, respectively; V_0 and V are the initial volume and the volume when the displacement reaches x, respectively. Therefore, $V_0 = L_0 A_0$ and $V = L_x A_0 (1-\varepsilon)$, where L_0 and A_0 are the initial length and cross-sectional area of specimens, respectively; L_x and ε are the specimen length and the strain at displacement x, respectively. The pressure P can then be calculated by

$$P = P_0 \cdot \frac{1-\delta}{1-\varepsilon} \tag{6}$$

Since δ is a function of crushing time, t', differentiating Eq. (6) with respect to t' and taking $\dot{\varepsilon} = v / L_0 = \partial\varepsilon / \partial t'$, we obtain,

$$\dot{P} = \frac{P_0}{1-\varepsilon}\left(\frac{1-\delta}{1-\varepsilon}\cdot\dot{\varepsilon} - \dot{\delta}\right) \tag{7}$$

or

$$\dot{\delta} = \frac{1}{P_0}\left[P\dot{\varepsilon} - (1-\varepsilon)\dot{P}\right] \tag{8}$$

where $\dot{P} = \partial P / \partial t'$ and $\dot{\delta} = \partial\delta / \partial t'$. It can be seen that the changing rate of the leakage and the air pressure are both related to the strain rate and the strain. Since $\dot{P} = \frac{\partial P}{\partial t'} = \frac{\partial P}{\partial \varepsilon}\frac{\partial \varepsilon}{\partial t'} = \frac{\partial P}{\partial \varepsilon}\dot{\varepsilon}$, Eq. (8) can be re-written into another form, which is

$$\frac{\partial P}{\partial \varepsilon} - \frac{1}{1-\varepsilon}P = -\frac{P_0\dot{\delta}}{\dot{\varepsilon}}\cdot\frac{1}{1-\varepsilon} \tag{9}$$

For the purpose of simplification, the leakage of air has been assumed to be uniform, as assumed by Zhang and Yu [16]. Since the strain rate is constant, Eq. (9) is a first-order linear differential equation, which has a general solution,

$$P = e^{-\int \frac{-1}{1-\varepsilon} d\varepsilon} \cdot \left[C + \int (-\frac{P_0 \dot{\delta}}{\dot{\varepsilon}} \cdot \frac{1}{1-\varepsilon}) e^{\int (\frac{-1}{1-\varepsilon}) d\varepsilon} d\varepsilon \right] \tag{10}$$

i.e.,

$$P = \frac{1}{1-\varepsilon} \left(C - \frac{P_0 \dot{\delta}}{\dot{\varepsilon}} \cdot \varepsilon \right) \tag{11}$$

By considering the initial condition that $P=P_0$ at $\varepsilon=0$, it is found that $C=P_0$. Hence, Eq. (11) becomes

$$P = \frac{P_0}{1-\varepsilon} \left(1 - \frac{\dot{\delta}}{\dot{\varepsilon}} \cdot \varepsilon \right) \tag{12}$$

Comparing Eqs. (12) and (7) leads to $\delta = (\dot{\delta} / \dot{\varepsilon})\varepsilon$. It can be seen from Eq. (7) that $\delta<\varepsilon$ since $P>P_0$, so that $\dot{\delta} < \dot{\varepsilon}$. The change of pressure during the crush is

$$\Delta P = P_0 \cdot \left(\frac{1}{1-\varepsilon} - 1 \right) \cdot (1 - \frac{\dot{\delta}}{\dot{\varepsilon}}) \tag{13}$$

In Eq. (13), the only unknown parameter to be determined is $\dot{\delta}$, which can be fitted by experimental results. Stresses for two honeycomb specimens, one with a hole percentage, η, of 100% and one <100% at the same strain rate, will have the following relationship

$$\sigma_{100\%} = \sigma_{\eta} - \Delta P \tag{14}$$

By selecting a proper $\dot{\delta}$ value to obtain ΔP in Eq. (14), the stress-strain curves for the two tests will be coincident. A sample calculation is demonstrated in Fig. 9(a) for honeycomb specimens with η =51%. Taking $\dot{\delta}$ =40 s^{-1} and subtracting the calculated value of ΔP, the adjusted stress-strain curve had a good agreement with that for the specimen with 100% holes. All the $\dot{\delta}$ values can then be fitted through this method. It has been found that $\dot{\delta}$ is related to hole percentage and strain rate, but independent of the *t*/*l* ratio under the present experimental conditions. All the $\dot{\delta}$ values are listed in

Table 6 and plotted against the strain rate in Fig. 9(b). Using $y = a + bx^c$ to fit the data, empirical relations are obtained for specimens with different percentages of holes as plotted in Fig. 9(b). It can be seen that the leaking rate is almost independent of strain rate when the strain rate is below 1 s^{-1}, while it is dependent on the strain rate when $\dot{\varepsilon}$ >1 s^{-1}, and strongly so above 10 s^{-1}. Furthermore, specimens with more holes have a larger leaking rate. It should be mentioned that the two empirical relations shown in Fig. 9(b) can only satisfactorily predict the $\dot{\delta}$ values when the strain rate is larger than 10 s^{-1} because the fitting error is too big for those data points under low strain rate compression.

Using Eq. (12) and the obtained data in Table 6, the relationship between air pressure, strain and strain rate is plotted in Fig. 10. When the strain rate is 10^{-1} s^{-1}, the curves in Figs. 10(a) and (b) are horizontal straight lines, i.e., the strain exhibits no effect on the air pressure. For any strain rate above 10^{-1} s^{-1}, on the one hand, in order to achieve the same internal air pressure, e.g. 0.2 MPa, in the specimens under out-of-plane crushing, less strain would be required for higher strain rate compression, i.e., $\varepsilon_1 < \varepsilon_2 < \varepsilon_3$ and $\varepsilon_1^{'} < \varepsilon_2^{'} < \varepsilon_3^{'}$ for strain rates 10^2, 10 and 1 s^{-1}, respectively. On the other hand, less strain would be required for specimens without holes to achieve the same air pressure, e.g. 0.2 MPa, compared with those with 51% holes when the strain rate is fixed.

3.3 Strength enhancement caused by other factors

Three types of stress-strain curve are observed in Figs. 4-6 and they are summarised in Fig. 11. For quasi-static compression, the plateau region is flat for honeycombs with and without holes (Case 1). For dynamic compression, the plateau region is also flat for honeycombs with 100% holes (Case 2) but exhibits a gradient increase for honeycombs with 0% and 51% holes (Case 3, apparent strain hardening). It is evident that the apparent strain hardening of honeycombs under dynamic compression is mainly attributed to the pressure increase of the entrapped air, rather than a

contribution from hardening of the metal as previously discussed. Therefore, apart from the pressure increase caused by the entrapped air, the strength enhancement may also be attributed to other factors such as the strain rate sensitivity of cell wall material, the micro-inertia effect of the entrapped air and the effect of shock wave (for high velocity impact only). Those kinds of strength enhancement are independent of the strain in the plateau region under dynamic compression. Considering the empirical Eq. (4) for honeycomb with 100% holes (i.e., without the entrapped air effect), the stress is dependent on the t/l ratio and strain rate but independent of strain. In the plateau region, the stress without considering the entrapped air effect, σ_r, can then be treated as the same value with the mean plateau stress for honeycombs with 100% holes; that is,

$$\sigma_r = \sigma_{pl}^{*} = C_1 \sigma_{ys} (t/l)^{k_3} (1 + C_2 \dot{\varepsilon})^{p} \tag{15}$$

Therefore, the dynamic stress, σ_d, can be calculated by

$$\sigma_d = \sigma_r + \Delta P \tag{16}$$

From Eqs. (13), (15) and (16), dynamic stress-strain curves can be predicted from quasi-static tests. A sample calculation has been conducted for honeycomb 3.1-3/16-5052-.001N as shown in Fig. 12 (a). C_1, C_2, k_3, p and $\dot{\delta}$ used here are 4.26, 5.57, 1.55, 0.033 and 8 s^{-1} (values in Tables 5 and 6 for H31 with 100% holes), respectively. It is verified that the predicted plateau region has a good agreement with the experimental results. Similar agreement is also seen in Figs. 12 (b) and (c) for honeycomb 4.5-1/8-5052-.001N and 8.1-1/8-5052-.002N using corresponding parameters listed in Tables 5 and 6. This confirms that the strain hardening of honeycombs is caused by the pressure change during the crushing. Furthermore, Eqs. (15) and (16) indicate that the stress was also dependent on the t/l ratio by a power relation, which explains the phenomenon described in Section 3.2 and in Figs. 7 and 8 whereby the t/l ratio affects the strength enhancement during crushing. However, this is not influenced by the entrapped air pressure. It is important to

note that the solid lines in Fig. 12 are prediction of the plateau region only, and not the steep rise into the densification at high strain.

3.4 The effect of the honeycomb geometry

In order to study the effect of honeycomb geometry on the dynamic properties of honeycombs, honeycomb 4.2-3/8-5052-.003N was selected as having the same *t*/*l* ratio as 4.5-1/8-5052-.001N but larger *t* and *l*. The stress-strain curves for all the tests are shown in Fig. 13. Similar trend as those in Figs. 4-6 can be seen. Using the previous fitting method, the obtained $\dot{\delta}$ shares the same values as honeycomb 4.5-1/8-5052-.001N, which indicates that $\dot{\delta}$ is independent of the honeycomb geometry. However, the plateau stress for this honeycomb is slightly lower than that of the honeycomb 4.5-1/8-5052-.001N as listed in Table 3, even though they have the same *t*/*l* ratio. This might be caused by the different manufacturing technique. According to the data provided by the manufacturer, the density is slightly lower than 4.5-1/8-5052-.001N (72.09 compared with 67.28 kg/m^3), which could be the reason for the lower plateau stress. This provides a possible scheme of using large cell size honeycombs in a more dedicated study, e.g. a study of the buckling of honeycomb cell wall and its wave length.

3.5 Deformation pattern

Digital and high speed cameras were used to observe the deformation and bucking patterns of honeycombs during the quasi-static and high rate compression tests, respectively. During the crush, plastic collapse was found to start from the interface between the honeycomb specimen and the support without exception. No other deformation pattern was found in all the tests, which was quite different from the observations in the parallel study [13]. In the parallel study, the buckling might shift from one interface to another during the high rate compression and might end in the

middle region of the specimens. Typical images for honeycomb 4.2-3/8-5052-.003N have been chosen for Fig. 14 because of its a larger cell size. This one-way buckling pattern might be explained by the stress concentration in the interface region attached to the support, where a strong constraint existed due to the holes and the adhesive. However, the different buckling patterns found earlier [13] did not appear to produce a measurable different stress-strain curve. It is therefore concluded that the location of the start of buckling has no significant influence on the measured stress-strain curve reported here.

It was also observed that, during high rate compression, abundant debris flew out of the specimen without holes, though it cannot be seen in Fig. 14 (c) due to resolution limitation. However, for those specimens with 100% holes, very few debris were found, which also occurred in the quasi-static and low rate tests. For specimens without holes, under high rate compression, there were limited holes and gaps for the entrapped air to escape. Therefore, the pressure of the air might become very high and burst through, releasing debris caused by damage to the EP 280 glue. However, for the specimens with holes or those under quasi-static and low rate compression tests, the air had sufficient time to escape and, consequently, the pressure built up in the air was much lower.

The half wave length of the plastic buckling is a key parameter to characterize honeycomb properties. According to Wierzbicki's study [19], for hexagonal honeycombs, $\lambda = 0.821\sqrt[3]{tl^2}$. Since all the selected honeycombs have relatively small cell size, the half wavelength of specimens in the present study is small. The measured 2λ were approximately 1.9 mm, 1.5 mm, 1.7mm and 5.0 mm for H31, H45, H81 and H42, respectively. These values are all higher than the values predicted by Wierzbicki's equation. Zhang and Yu [16] found the decrease of half wavelength caused by the increased air pressure and the changing of folding mode from diamond to ring mode when the pressure was larger than 0.5 MPa. Unfortunately, no change in wave length has been found in the present study. The reason might be that the smaller pressure increase, approximately 0.2 MPa at the

end of the crushing, could not produce a detectable change of wavelength. It is technically difficult to apply the experimental method proposed in [16] to our Instron high rate test system and honeycombs, so as to achieve a larger pressure change.

3.6 Remarks on the constitutive relation for honeycombs under dynamic out-of-plane crushing

In industrial design and numerical modelling, constitutive models are of great importance. Numerous analytical and empirical constitutive models for cellular materials have been proposed under quasi-static and dynamic loadings. Gibson and Ashby [1] summarized the major models in their book. In the elastic region, the relationship between Young's modulus and the t/l ratio has been extensively studied. However, the plastic buckling region is of the most interest because of the energy absorption contribution for honeycomb structures. The plastic buckling under quasi-static crushing has been widely studied. McFarland [20] developed a structure subjected to axial loading and found a solution to calculate the mean crush stress. Wierzbicki [19] analytically studied the crush of metal honeycombs and also gave a prediction of the mean crushing force. In their study on pressurized tubes, Zhang and Yu [16] proposed an empirical equation to predict the crushing force in relation to the displacement. Cowper and Symonds [21] developed an empirical equation for strain rate sensitive materials. Reid and Peng [22] studied the dynamic axial crushing of wood and proposed a shock theory to calculate the mean crushing force. However, most of the study focused on the evaluation of mean crushing force or stress, which is not related to strain. Detailed constitutive relations to predict the stress-strain relation for honeycombs under quasi-static or dynamic compressive loadings are still limited. The present study has revealed that the apparent strain hardening of honeycombs is mainly due to the increase of entrapped air pressure during the dynamic crushing. By adding the air effect defined by Eq. (14), an entire constitutive relation could

be constructed. Rewriting Eq. (16), the relationship between the stress, σ, the strain and the strain rate in the plateau region can be described as

$$\sigma = C_1\sigma_{ys}(t/l)^{k_3}(1+C_2\dot{\varepsilon})^p + P_0 \cdot \left(\frac{1}{1-\varepsilon}-1\right)\cdot(1-\frac{\dot{\delta}}{\dot{\varepsilon}}), \quad (17)$$

where C_1, C_2, k_3, p and $\dot{\delta}$ are values listed in Tables 5 and 6.

4. Conclusions

Using a specially designed testing technique, the effect of entrapped air on the strength enhancement of honeycombs with different *t*/*l* ratios subjected to out-of plane crushing at various strain rates was studied. It has been found that the mean plateau stress was dependent on the *t*/*l* ratio and strain rate. An empirical relation is proposed to evaluate the mean plateau stress.

An analytical solution is then developed to study the effect of the entrapped air by introducing a leaking rate, $\dot{\delta}$. It is shown that $\dot{\delta}$ is dependent on the strain rate and hole percentage, and independent of *t*/*l* ratio and cell size. The strength increase due to the pressure increase in relation to the strain rate has been quantified and the corresponding $\dot{\delta}$ values experimentally fitted. It is also verified that the stress is independent of the strain for honeycombs with 100% holes, i.e. these honeycombs behave like ideal elastic-perfectly plastic materials in the elastic and plateau regions. The strain hardening of honeycombs during the dynamic crushing is mostly due to pressure developed by entrapped air.

The deformation pattern for honeycombs under dynamic crushing was a one-way buckling, i.e. starting from the bottom of the specimens, which is believed to be a result of the strong constraint at the bottom caused by holes and the adhesive.

In order to predict the dynamic response of honeycombs based on their quasi-static tests, a precise constitutive relation is required. The present study provides valuable evidence for the strength enhancement caused by the entrapped air in the dynamic crushing of honeycombs.

Acknowledgements

The authors are grateful to the Cooperative Research Centre for Advanced Automotive Technology (AutoCRC) for the financial support through a postgraduate scholarship and to Swinburne University of Technology. The fourth author (T.X. Yu) would like to thank the support from the Key Project No. 11032001 under the National Natural Science Foundation of China.

References

[1] L.J. Gibson, M.F. Ashby, Cellular solids - structure and properties, 2nd ed., Cambridge University Press, 1997.

[2] G. Lu, T.X. Yu, Energy absorption of materials and structures, Woodhead Publishing Limited, Cambridge, 2003.

[3] T. Mukai, H. Kanahashi, T. Miyoshi, M. Mabuchi, T.G. Nieh, K. Higashi, Experimental study of energy absorption in a close-celled aluminum foam under dynamic loading, Scripta Mat., 40 (1999) 921-927.

[4] K.A. Dannemann, J. Lankford, High strain rate compression of closed-cell aluminium foams, Mater. Sci. Eng., A, 293 (2000) 157-164.

[5] T. Mukai, T. Miyoshi, S. Nakano, H. Somekawa, K. Higashi, Compressive response of a closed-cell aluminum foam at high strain rate, Scripta Mat., 54 (2006) 533-537.

[6] S. Xu, D. Ruan, J. Beynon, G. Lu, Experimental investigation of the dynamic behavior of aluminum foams, Material. Sci. Forum, 654-656, (2010) 950-953.

[7] A. Paul, U. Ramamurty, Strain rate sensitivity of a closed-cell aluminum foam, Mater. Sci. Eng., A, 281 (2000) 1-7.

[8] V.S. Deshpande, N.A. Fleck, High strain rate compressive behaviour of aluminium alloy foams, Int. J. Impact Eng., 24 (2000) 277-298.

[9] D. Ruan, G. Lu, F.L. Chen, E. Siores, Compressive behaviour of aluminium foams at low and medium strain rates, Compos. Struct., 57 (2002) 331-336.

[10] W.E. Baker, T.C. Togami, J.C. Weydert, Static and dynamic properties of high-density metal honeycombs, Int. J. Impact Eng., 21 (1998) 149-163.

[11] W. Goldsmith, G.T. Wang, K. Li, D. Crane, Perforation of cellular sandwich plates, Int. J. Impact Eng., 19 (1997) 361-379.

[12] H. Zhao, G. Gary, Crushing behaviour of aluminium honeycombs under impact loading, Int. J. Impact Eng., 21 (1998) 827-836.

[13] S. Xu, J.H. Beynon, D. Ruan, G. Lu, Experimental study of the out-of-plane bynamic compression of hexagonal honeycombs, submitted to Compos. Struct., (2011).

[14] E. Wu, W.-S. Jiang, Axial crush of metallic honeycombs, Int. J. Impact Eng., 19 (1997) 439-456.

[15] H. Zhao, I. Elnasri, S. Abdennadher, An experimental study on the behaviour under impact loading of metallic cellular materials, Int. J. Mech. Sci., 47 (2005) 757-774.

[16] X.W. Zhang, T.X. Yu, Energy absorption of pressurized thin-walled circular tubes under axial crushing, Int. J. Mech. Sci., 51 (2009) 335-349.

[17] M. A. Dawson, G. H. McKinley, L. J. Gibson, The dynamic compressive response of open-cell foam impregnated with a Newtonian fluid, J. App. Mech., 75 (2008) 041015-1-11.

[18] Q.M. Li, I. Magkiriadis, J.J. Harrigan, Compressive strain at the onset of densification of cellular solids, J. Cell. Plast., 42 (2006) 371-392.

[19] T. Wierzbicki, Crushing analysis of metal honeycombs, Int. J. Impact Eng., 1 (1983) 157-174.

[20] R.K. FcFarland, Hexagonal cell structrures under post-buckling axial load, AIAA Journal, 1 (1963) 1380-1385.

[21] G.R. Cowper, P.S. Symonds, Strain hardening and strain rate effect in the impact loading of cantilever beams, Brown University, Division of Applied Mathematics, Technical Report 28 (1957).

[22] S.R. Reid, C. Peng, Dynamic uniaxial crushing of wood, Int. J. Impact Eng., 19 (1997) 531-570.

Highlights

The contribution of the entrapped air to the dynamic out-of-plane strength of aluminium honeycombs was studied experimentally and analytically by employing honeycombs containing different percentages of holes.

The dynamic out-of-plane strength enhancement of aluminium honeycombs is attributed to the increase of strain rate and the pressure change caused by the entrapped air.

Constitutive relation to describe the plastic collapse stress in relation to the t/l ratio, the strain and strain rate was proposed.

Figure 1

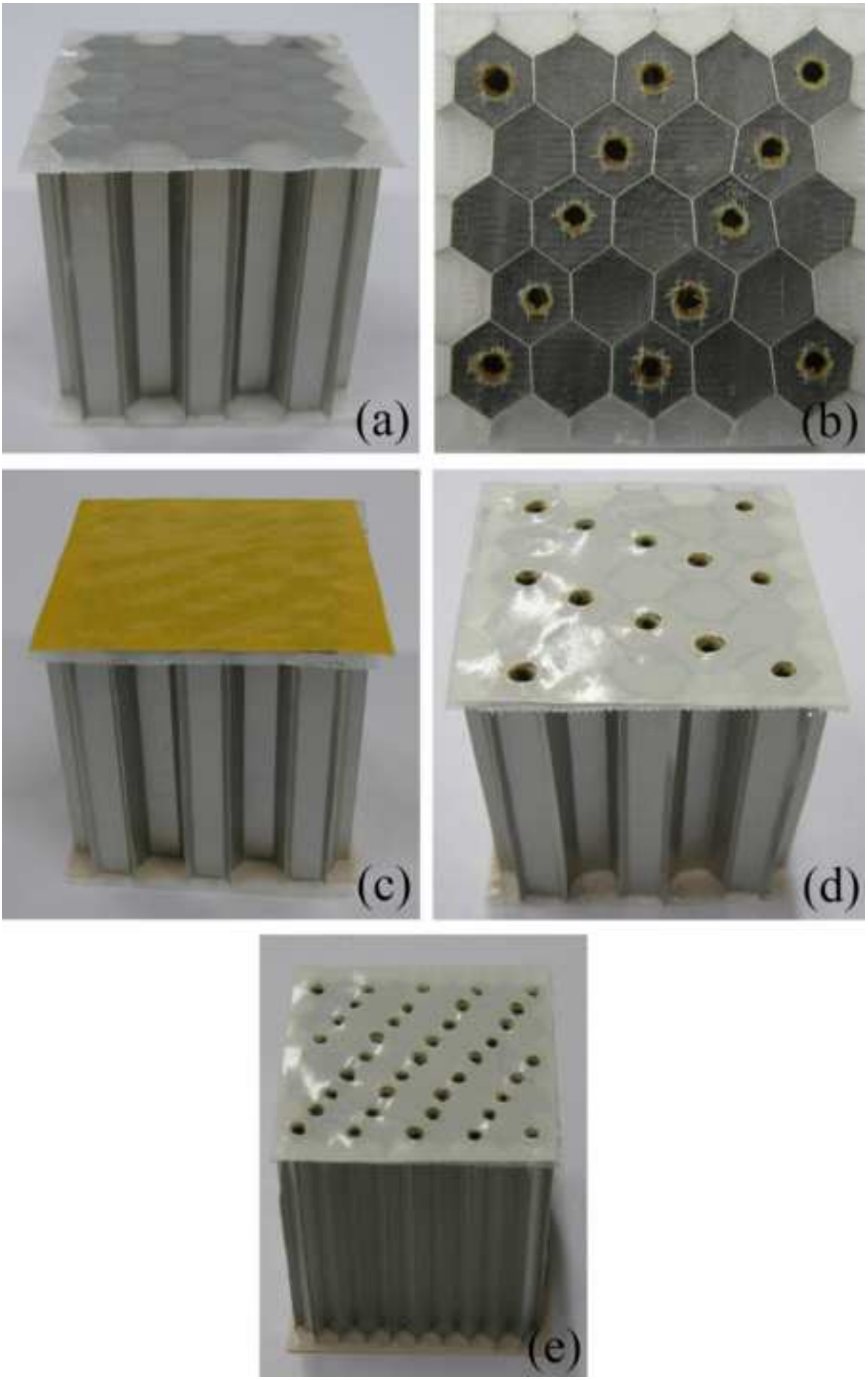

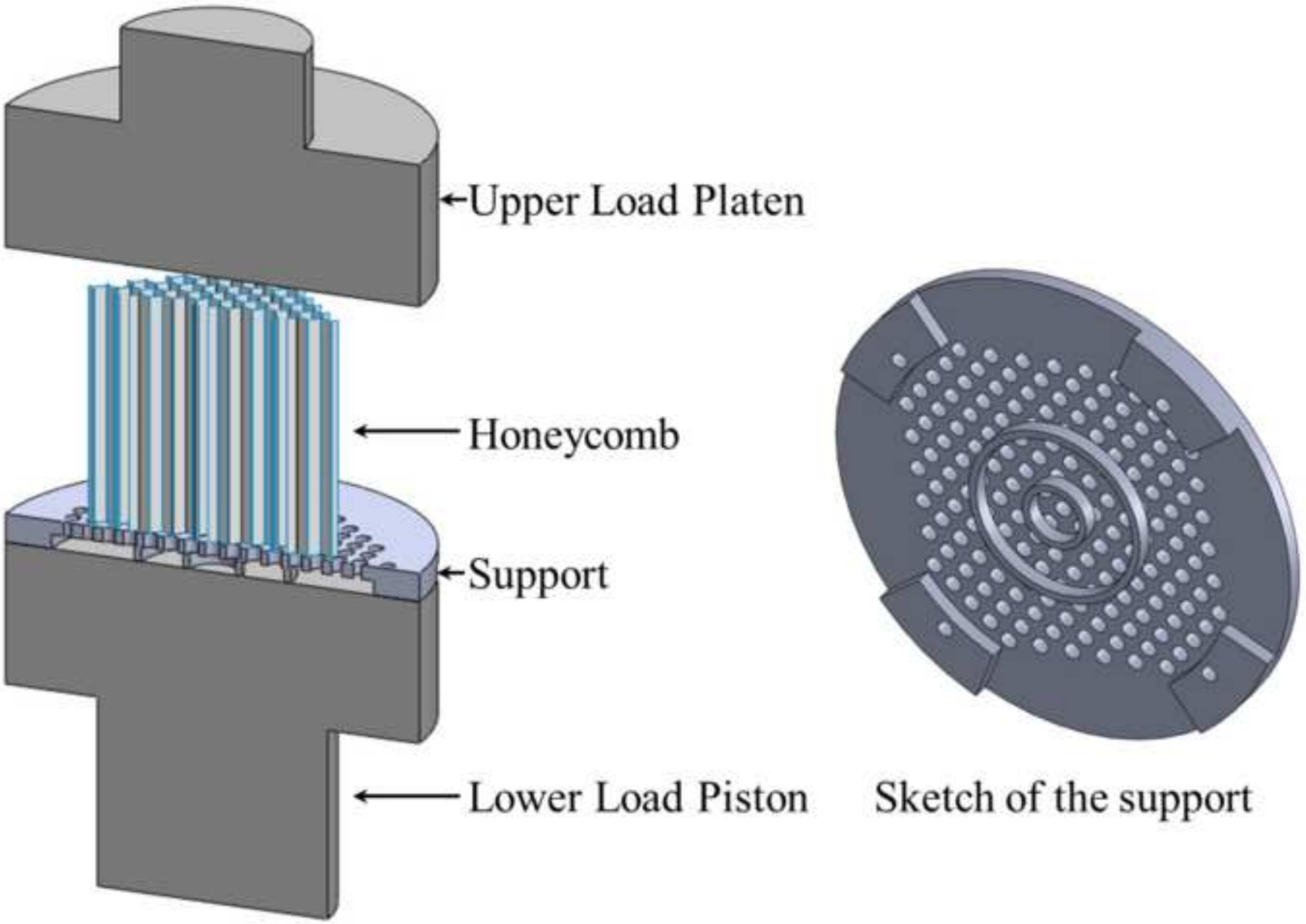

Figure 3

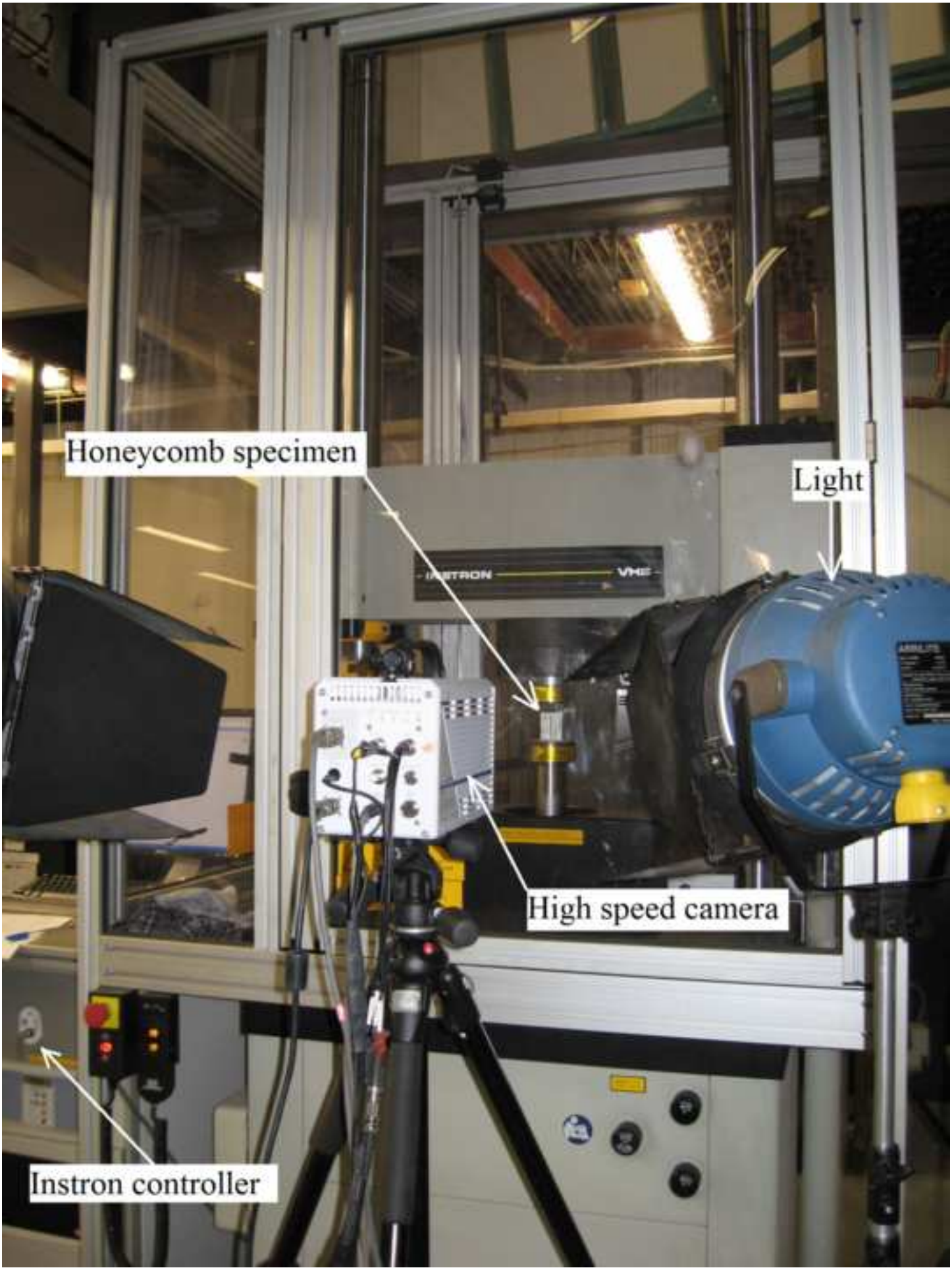

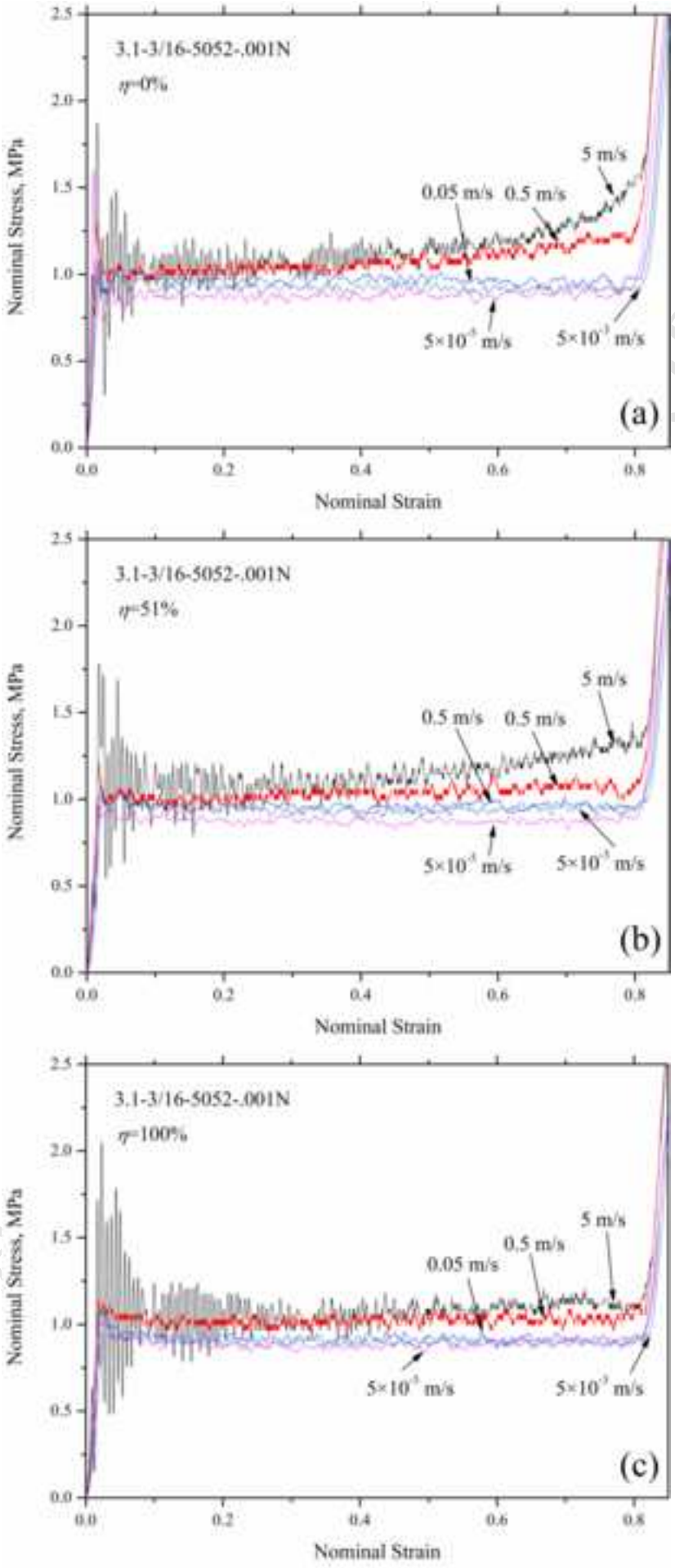

Figure 5

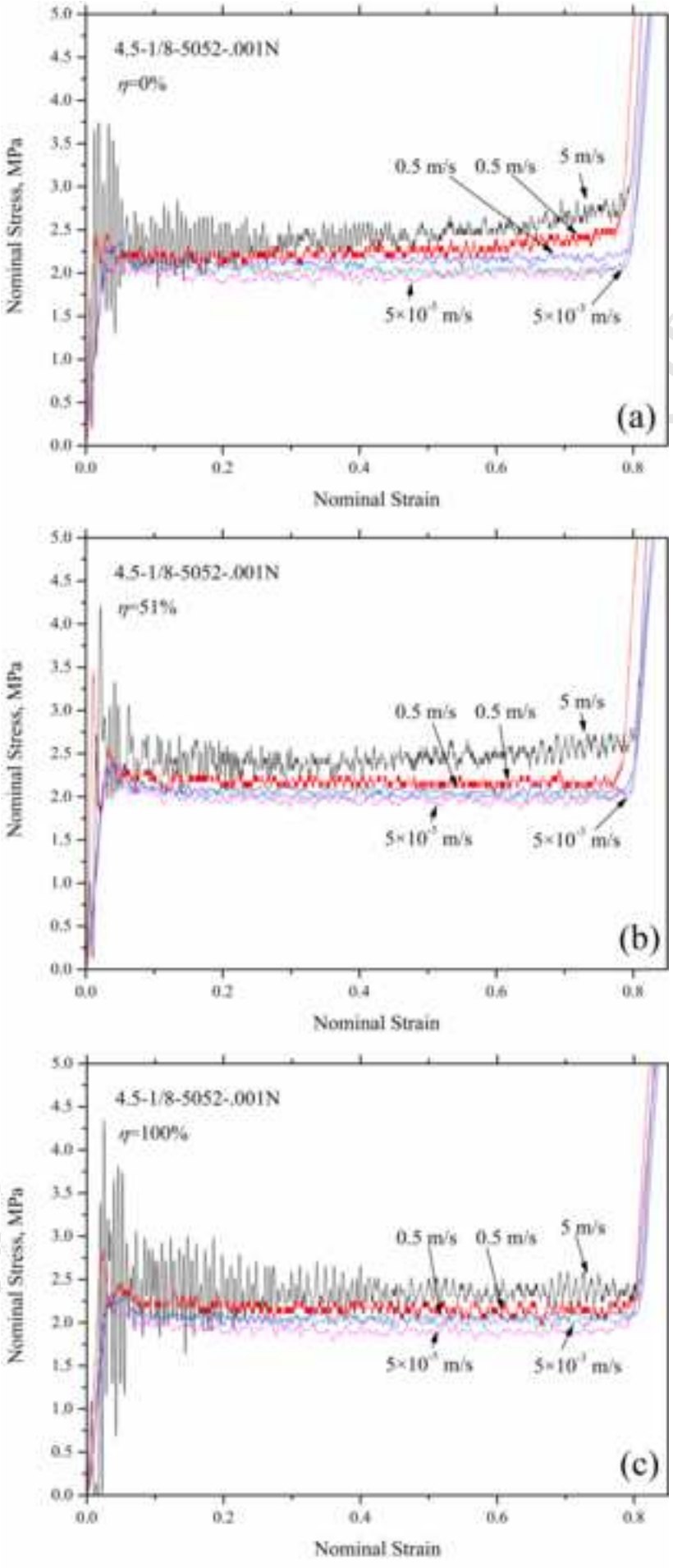

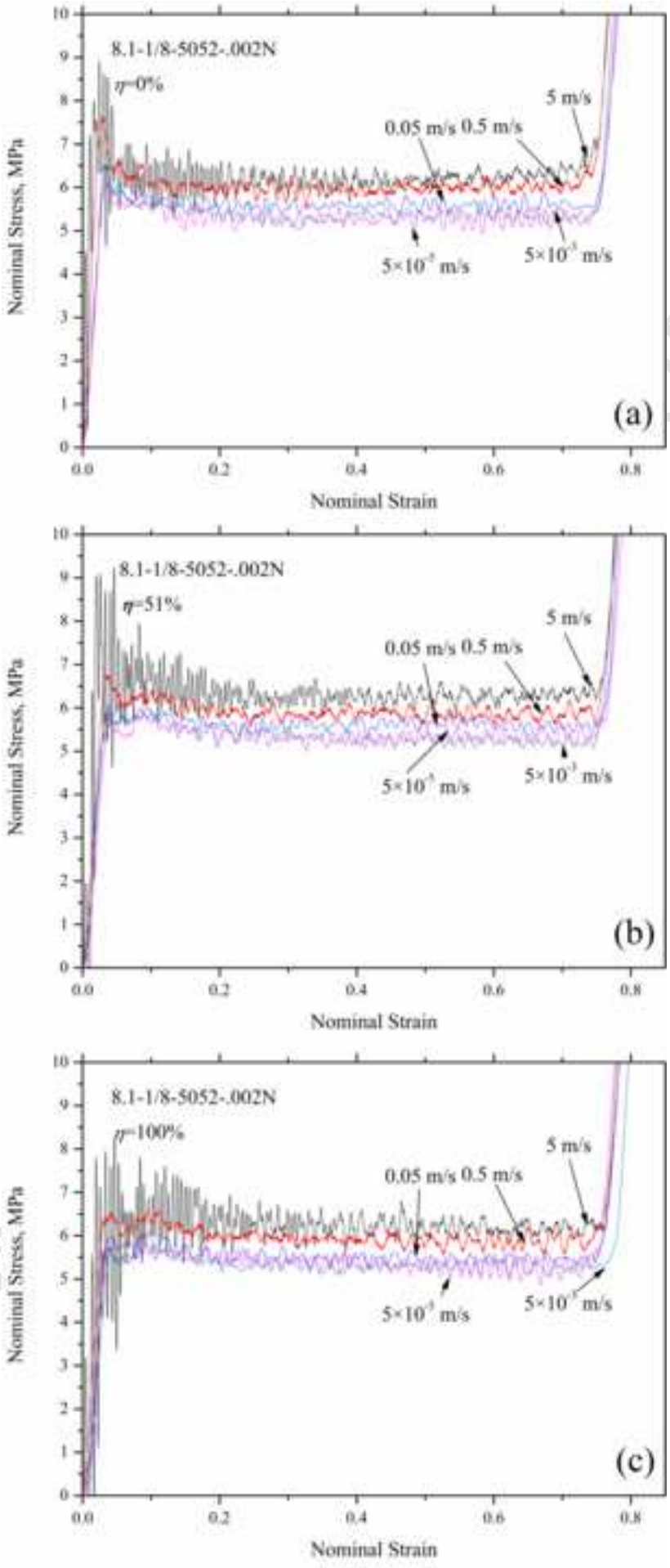

Figure 7
Click here to download high resolution image

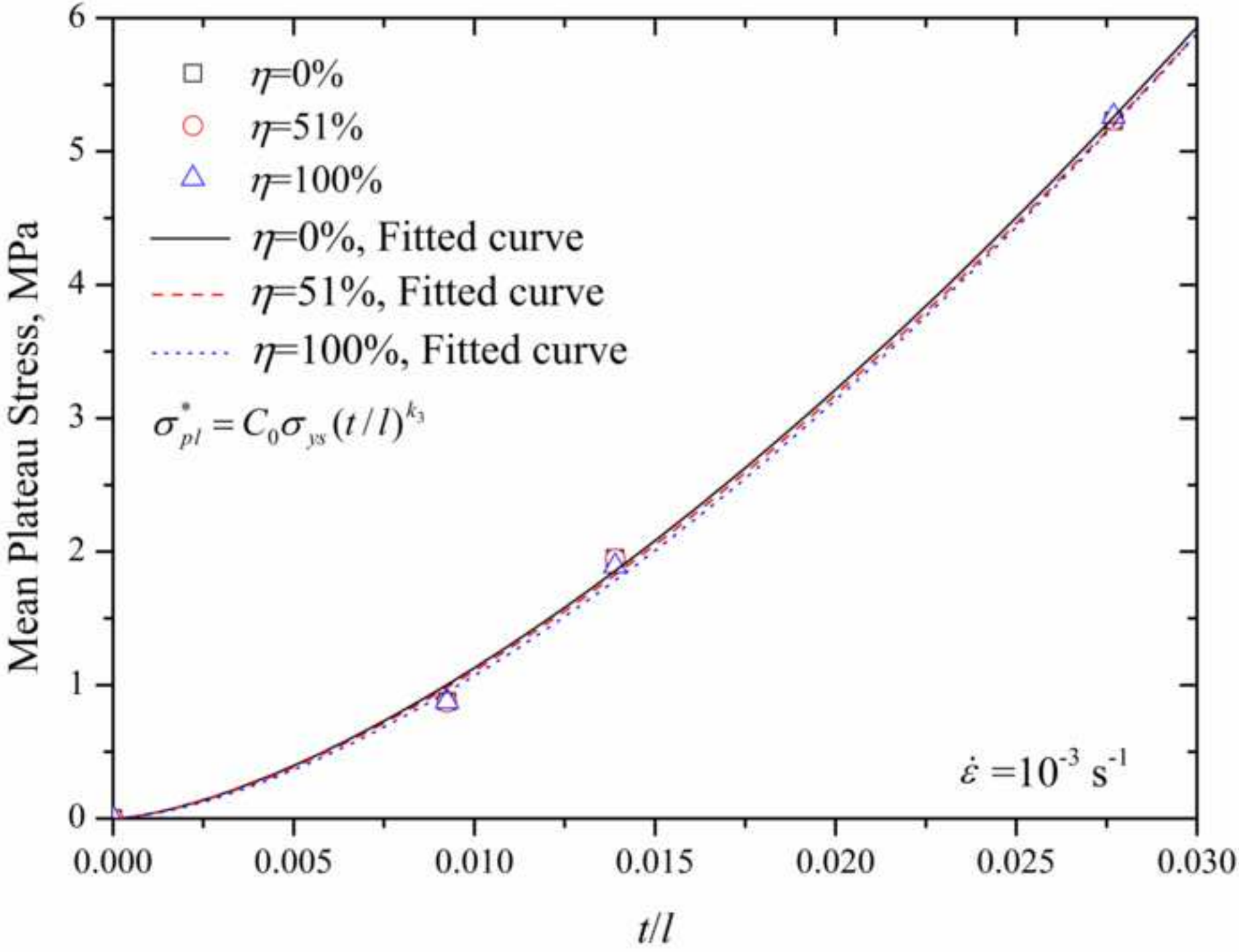

Figure 8

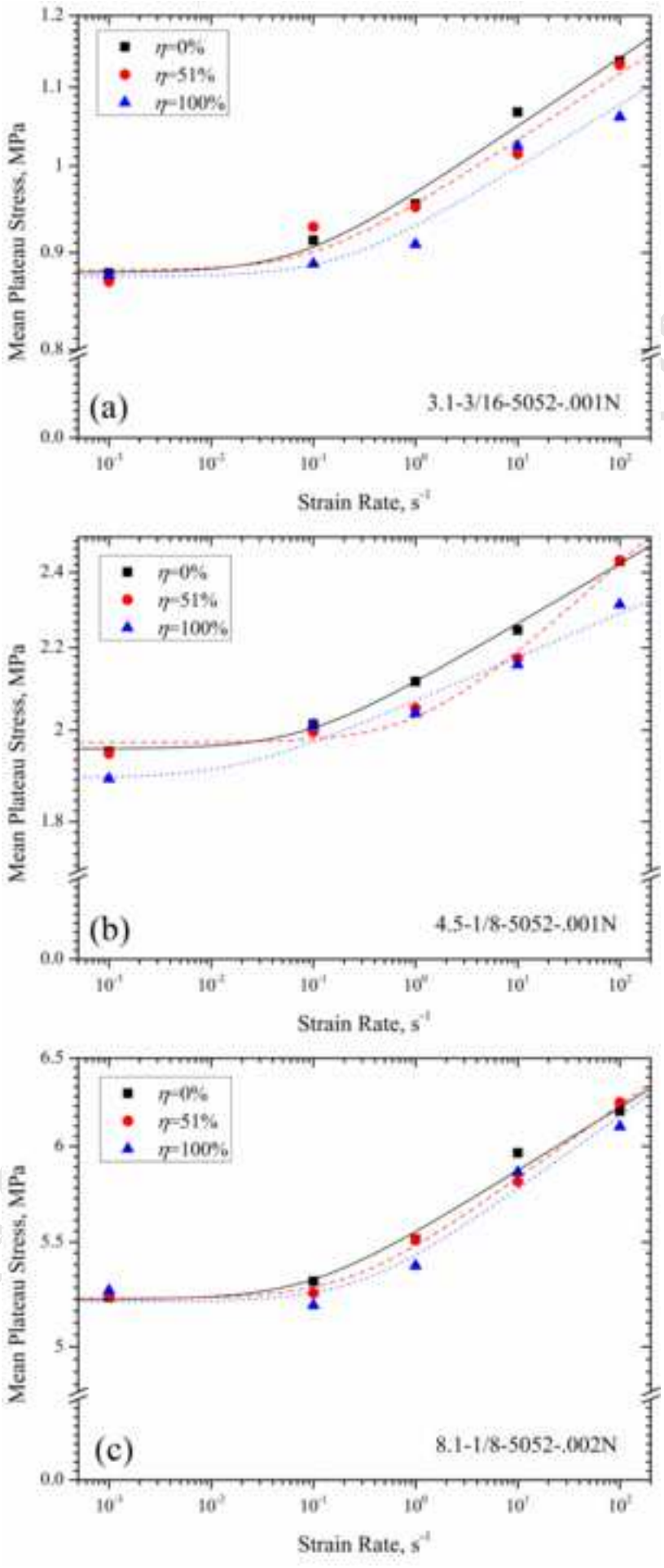

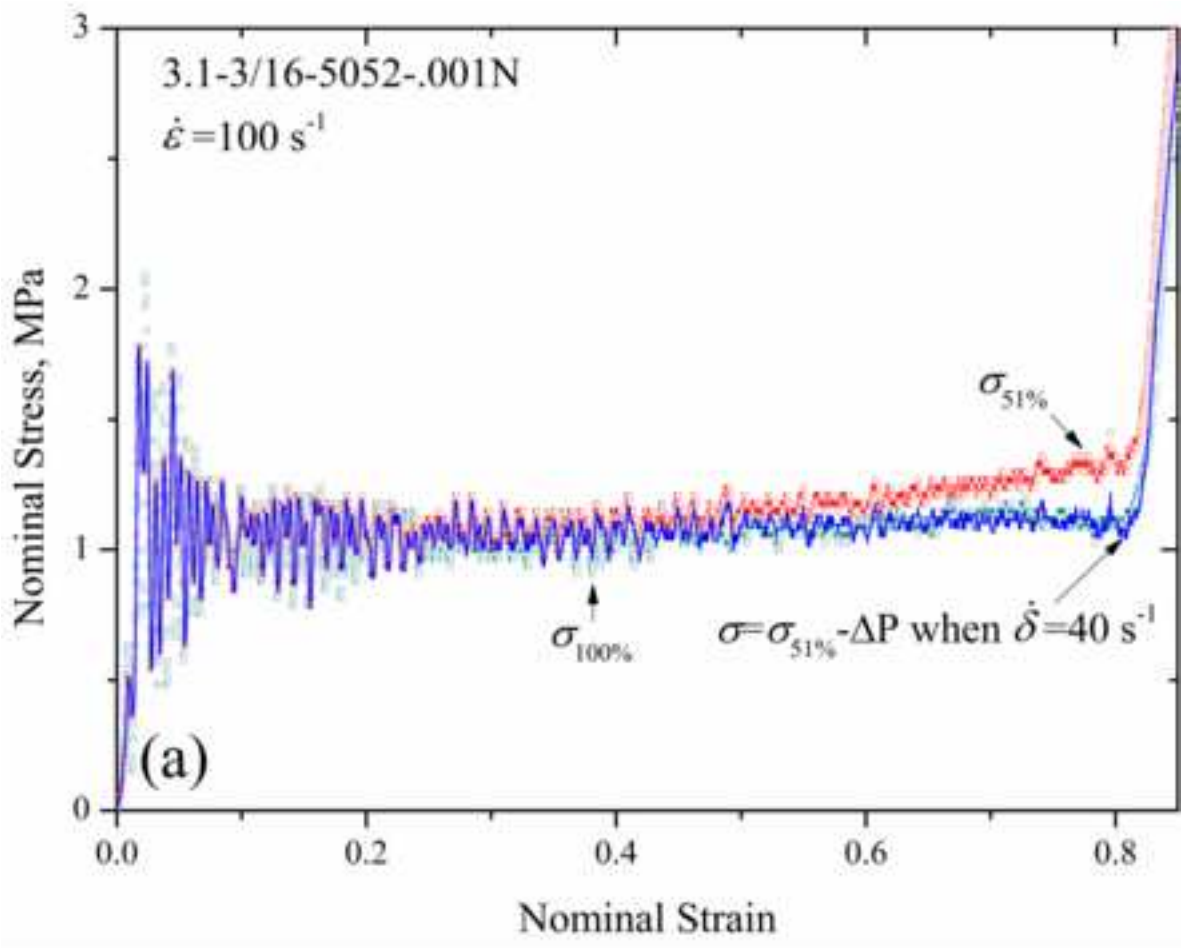

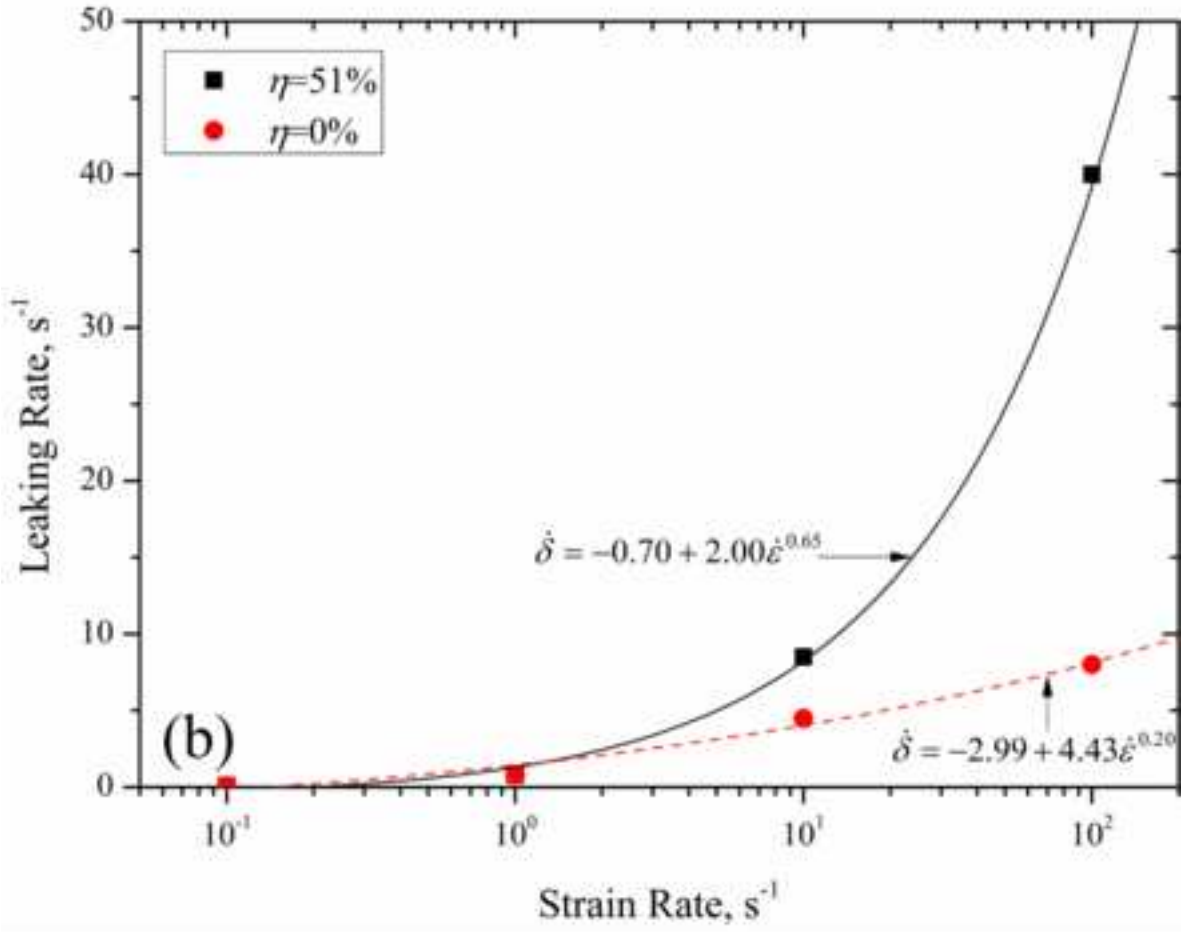

Figure 10

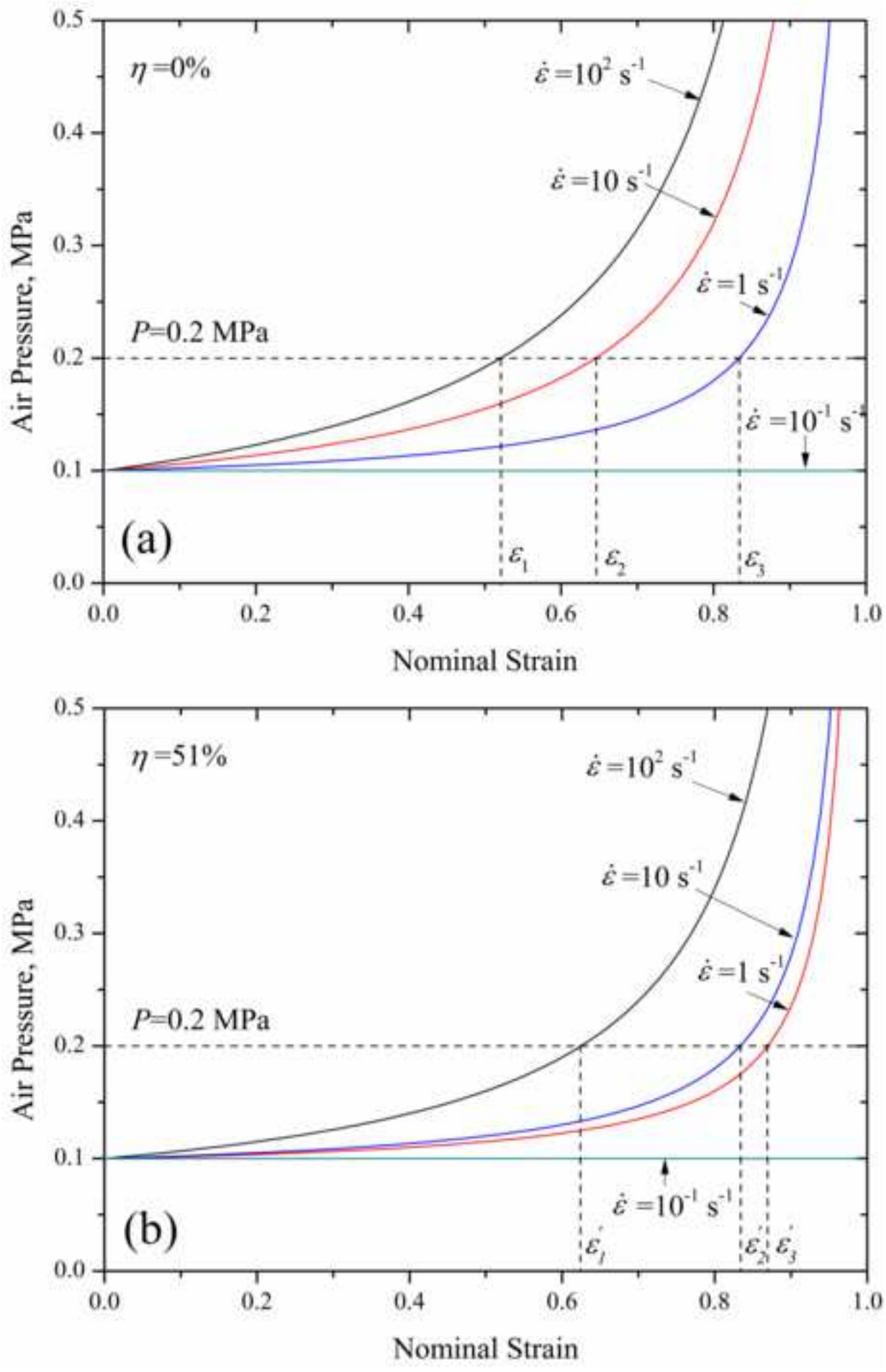

Figure 11
Click here to download high resolution image

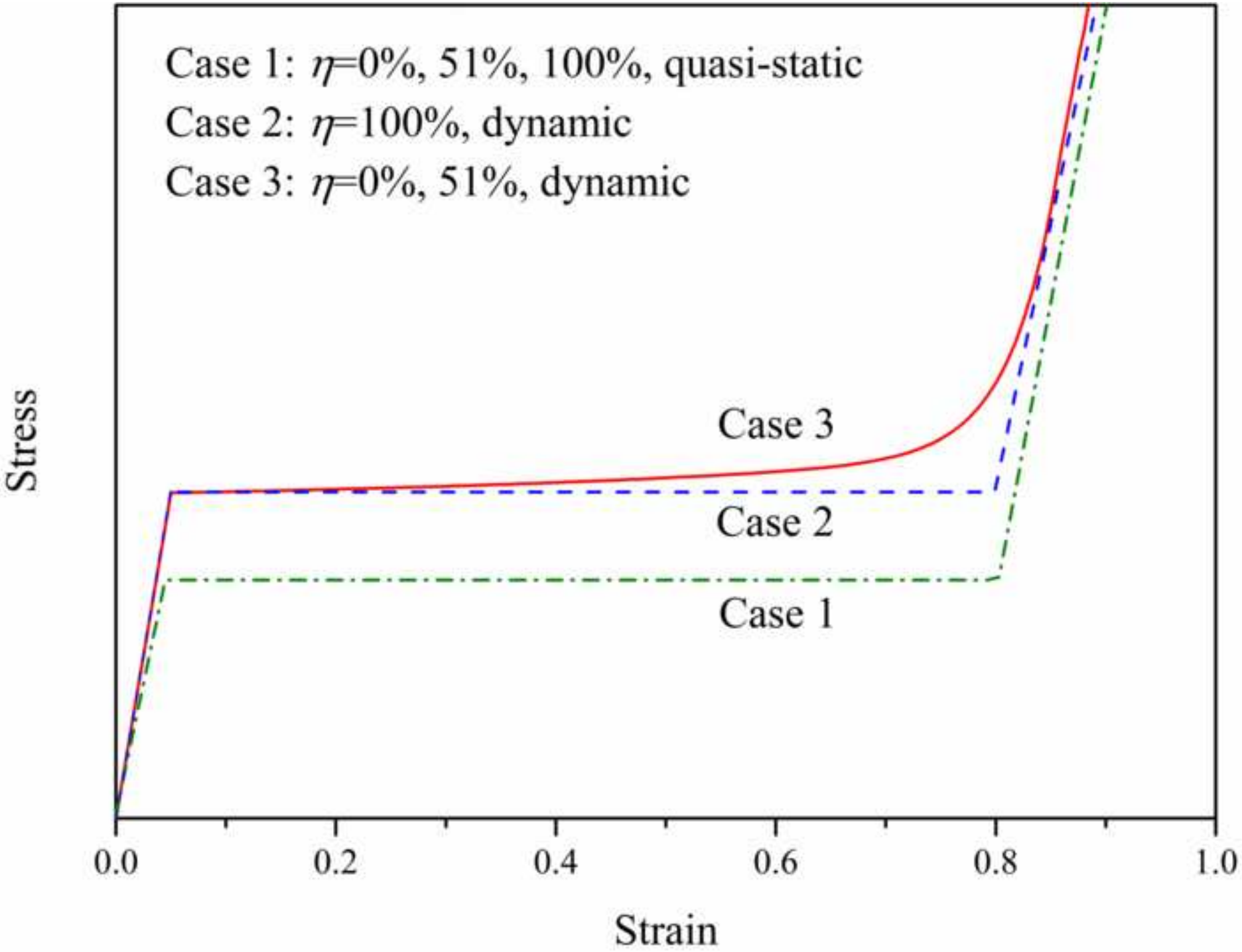

Figure 12

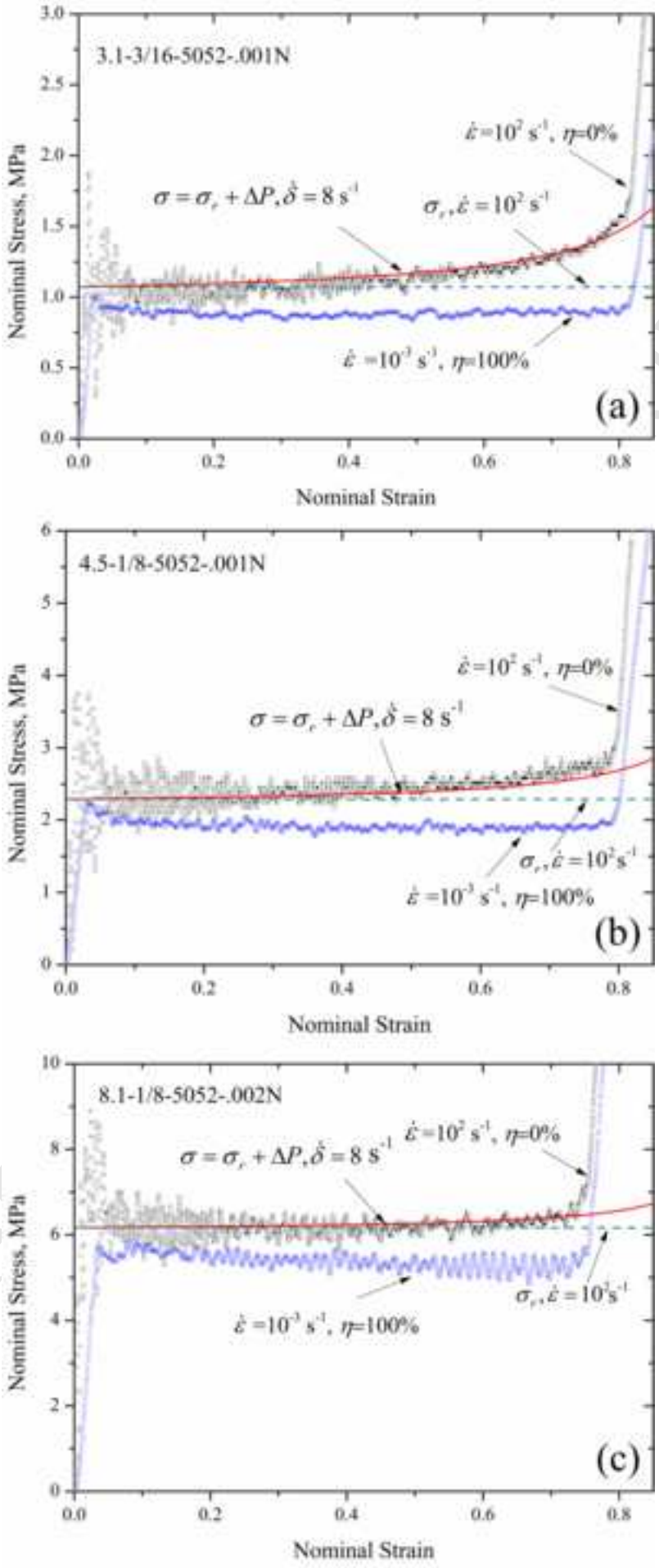

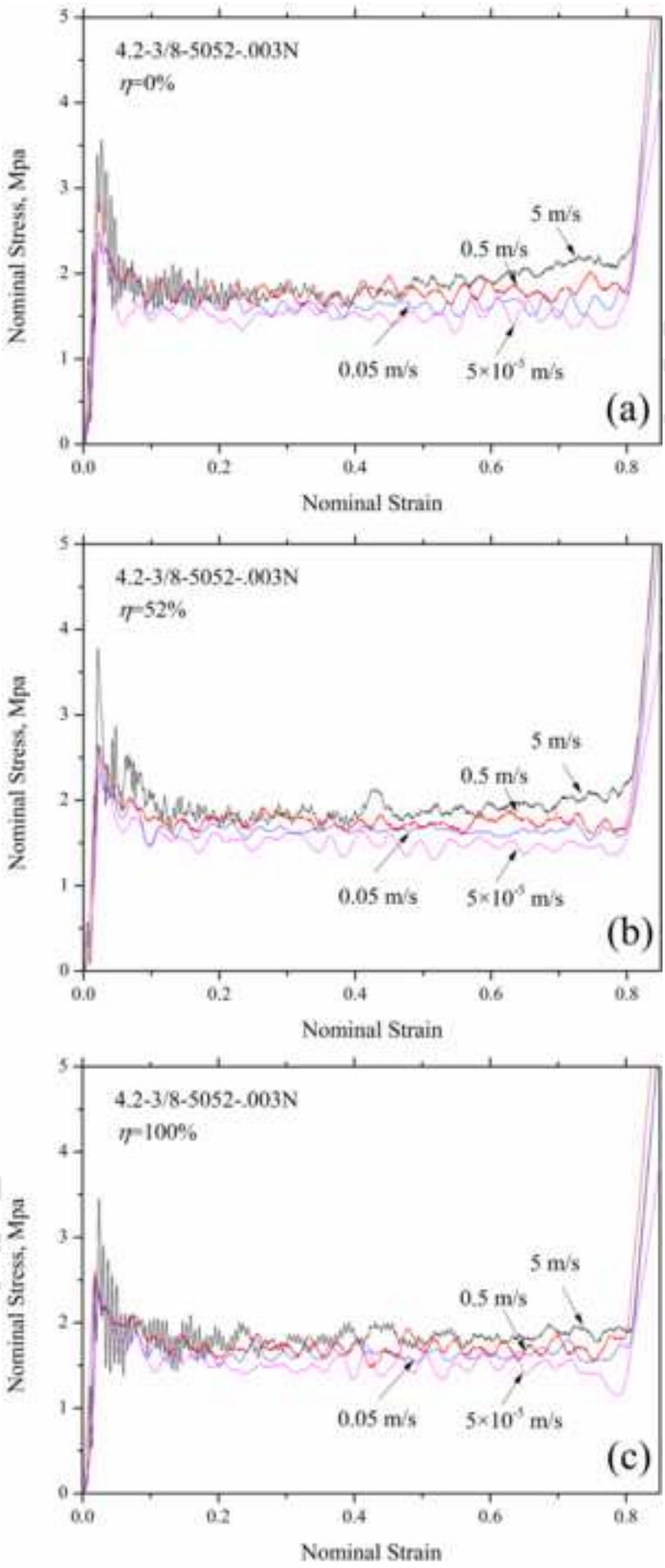

Table 1

Table 1. HexWeb® CR III 5052 aluminium hexagonal honeycomb

Designation	Nominal Density, ρ_s (kg/m^3)	c (mm)	t (mm)	Compressive					Crush Strength (MPa)
				Peak		Stabilized			
				Strength (MPa)		Strength (MPa)		Modulus(GPa)	
				typ	min	typ	min		
4.5-1/8-5052-.001N	72.09	3.175	0.0254	3.79	2.59	3.93	3.28	1.03	1.79
8.1-1/8-5052-.002N	129.75	3.175	0.0508	10.34	6.89	10.76	7.58	2.41	5.17
3.1-3/16-5052-.001N	49.66	4.763	0.0254	2.00	1.38	2.31	1.48	0.52	0.90
4.2-3/8-5052-.003N	67.28	9.525	0.0762	3.59	2.31	3.86	2.45	0.93	1.52

* In designation "4.5-1/8-5052-.001N", 4.5 is the nominal density in pounds per cubic foot, 1/8 is the cell size in inches, 5052 is aluminium alloy, .001 is the nominal foil thickness in inches and N indicates the cell walls are not perforated. "typ" is the typical value and "min" is the minimum value. (Data supplied by the manufacturer).

Table 2

Table 2. Properties of GMS Composites EP-280 films

Item	Flexural Strength, MPa (at 23 °C)	Ultimate Elongation, % (at 23 °C)	Flexural Modulus, MPa (at 23 °C)	Tg, °C (DSC,10K/min)	Interlaminar shear strength, MPa *
Value	146-156	6.0-7.0	3150-3400	102-108	62-66

*12 layers UD e-glass (425 gsm) 3.2 mm thick laminate

Table 3

Table 3. Summary of all the tests conducted by MTS and Instron machines

Test No.	Material*	Mass (mg)	Hole percentage (%)	t/l	ρ/ρ_0 (%)	Velocity (m/s)	Strain rate (s^{-1})	σ^*_{pl} (MPa)	ε_d
AE31-1-1	H31	4.7	0	0.00924	1.85	5	10^2	1.136	0.809
AE31-1-2	H31	4.6	10	0.00924	1.85	5	10^2	1.138	0.808
AE31-1-3	H31	4.7	51	0.00924	1.85	5	10^2	1.130	0.808
AE31-1-4	H31	4.6	100	0.00924	1.85	5	10^2	1.061	0.809
AE31-2-1	H31	4.7	0	0.00924	1.85	0.5	10	1.068	0.796
AE31-2-2	H31	4.7	10	0.00924	1.85	0.5	10	1.028	0.799
AE31-2-3	H31	4.7	51	0.00924	1.85	0.5	10	1.025	0.807
AE31-2-4	H31	4.7	100	0.00924	1.85	0.5	10	1.015	0.816
AE31-3-1	H31	4.6	0	0.00924	1.85	0.05	1	0.955	0.807
AE31-3-2	H31	4.7	51	0.00924	1.85	0.05	1	0.951	0.800
AE31-3-3	H31	4.7	100	0.00924	1.85	0.05	1	0.909	0.814
AE31-4-1	H31	4.7	0	0.00924	1.85	5×10^{-3}	10^{-1}	0.914	0.809
AE31-4-2	H31	4.7	51	0.00924	1.85	5×10^{-3}	10^{-1}	0.929	0.815
AE31-4-3	H31	4.7	100	0.00924	1.85	5×10^{-3}	10^{-1}	0.888	0.820
AE31-5-1	H31	4.7	0	0.00924	1.85	5×10^{-5}	10^{-3}	0.878	0.794
AE31-5-2	H31	4.7	51	0.00924	1.85	5×10^{-5}	10^{-3}	0.869	0.803
AE31-5-3	H31	4.6	100	0.00924	1.85	5×10^{-5}	10^{-3}	0.876	0.813
AE45-1-1	H45	3.2	0	0.0139	2.69	5	10^2	2.431	0.787
AE45-1-2	H45	3.3	51	0.0139	2.69	5	10^2	2.434	0.801
AE45-1-3	H45	3.2	100	0.0139	2.69	5	10^2	2.313	0.806
AE45-2-1	H45	3.3	0	0.0139	2.69	0.5	10	2.246	0.774
AE45-2-2	H45	3.2	51	0.0139	2.69	0.5	10	2.174	0.776
AE45-2-3	H45	3.3	100	0.0139	2.69	0.5	10	2.158	0.795
AE45-3-1	H45	3.3	0	0.0139	2.69	0.05	1	2.116	0.793
AE45-3-2	H45	3.3	51	0.0139	2.69	0.05	1	2.052	0.787
AE45-3-3	H45	3.2	100	0.0139	2.69	0.05	1	2.040	0.803
AE45-4-1	H45	3.3	0	0.0139	2.69	5×10^{-3}	10^{-1}	2.014	0.788
AE45-4-2	H45	3.3	51	0.0139	2.69	5×10^{-3}	10^{-1}	1.997	0.791
AE45-4-3	H45	3.3	100	0.0139	2.69	5×10^{-3}	10^{-1}	2.013	0.797
AE45-5-1	H45	3.3	0	0.0139	2.69	5×10^{-5}	10^{-3}	1.952	0.784
AE45-5-2	H45	3.3	51	0.0139	2.69	5×10^{-5}	10^{-3}	1.947	0.795
AE45-5-3	H45	3.2	100	0.0139	2.69	5×10^{-5}	10^{-3}	1.892	0.790
AE81-1-1	H81	5.9	0	0.0277	4.84	5	10^2	6.196	0.750
AE81-1-2	H81	5.9	51	0.0277	4.84	5	10^2	6.245	0.751
AE81-1-3	H81	5.9	100	0.0277	4.84	5	10^2	6.109	0.761
AE81-2-1	H81	5.9	0	0.0277	4.84	0.5	10	5.964	0.743
AE81-2-2	H81	5.9	51	0.0277	4.84	0.5	10	5.811	0.749
AE81-2-3	H81	5.9	100	0.0277	4.84	0.5	10	5.860	0.755
AE81-3-1	H81	5.9	0	0.0277	4.84	0.05	1	5.514	0.748
AE81-3-2	H81	5.9	51	0.0277	4.84	0.05	1	5.519	0.755
AE81-3-3	H81	5.9	100	0.0277	4.84	0.05	1	5.382	0.749
AE81-4-1	H81	5.9	0	0.0277	4.84	5×10^{-3}	10^{-1}	5.308	0.751
AE81-4-2	H81	5.9	51	0.0277	4.84	5×10^{-3}	10^{-1}	5.251	0.748
AE81-4-3	H81	5.9	100	0.0277	4.84	5×10^{-3}	10^{-1}	5.194	0.767
AE81-5-1	H81	5.9	0	0.0277	4.84	5×10^{-5}	10^{-3}	5.229	0.751
AE81-5-2	H81	5.9	51	0.0277	4.84	5×10^{-5}	10^{-3}	5.235	0.763
AE81-5-3	H81	5.9	100	0.0277	4.84	5×10^{-5}	10^{-3}	5.263	0.754
AE42-1-1	H42	8.8	0	0.0139	2.69	5	10^2	1.889	0.796
AE42-1-2	H42	9.0	52	0.0139	2.69	5	10^2	1.909	0.802
AE42-1-3	H42	9.1	100	0.0139	2.69	5	10^2	1.822	0.807
AE42-2-1	H42	9.0	0	0.0139	2.69	0.5	10	1.793	0.798
AE42-2-2	H42	9.1	52	0.0139	2.69	0.5	10	1.760	0.797
AE42-2-3	H42	9.0	100	0.0139	2.69	0.5	10	1.730	0.798
AE42-3-1	H42	8.9	0	0.0139	2.69	0.05	1	1.642	0.800
AE42-3-2	H42	9.0	52	0.0139	2.69	0.05	1	1.649	0.794
AE42-3-3	H42	8.9	100	0.0139	2.69	0.05	1	1.647	0.804
AE42-5-1	H42	9.0	0	0.0139	2.69	5×10^{-5}	10^{-3}	1.502	0.781
AE42-5-2	H42	9.0	52	0.0139	2.69	5×10^{-5}	10^{-3}	1.500	0.786
AE42-5-3	H42	9.0	100	0.0139	2.69	5×10^{-5}	10^{-3}	1.504	0.792

*H31: 3.1-3/16-5052-.001N; H45: 4.5-1/8-1/8-5052-.001N ; H81: 8.1-1/8-5052-.002N ; H42: 4.2-3/8-5052-.003N

Table 4

Table 4. Strength enhancement due to the increase of crushing velocity

Materials	Hole Percentage (%)	Plateau stress at $\dot{\varepsilon}=10^{-3}\ s^{-1}$(MPa)	Plateau stress at $\dot{\varepsilon}=10^{2}\ s^{-1}$(MPa)	Strength increase (MPa)	Difference (%)
H31	0	0.878	1.136	0.258	29.4
	51	0.869	1.130	0.261	30.0
	100	0.876	1.061	0.185	21.1
H45	0	1.952	2.431	0.479	24.5
	51	1.947	2.434	0.487	25.0
	100	1.892	2.313	0.421	22.3
H81	0	5.229	6.196	0.967	18.5
	51	5.235	6.245	1.01	19.3
	100	5.263	6.109	0.846	16.1

Table 5

Table 5. Fitted parameters for honeycomb specimens

Materials	η	C_0	C_1	C_2	k_3	p
H31	0%	4.05	3.55	13.89	1.51	0.036
	51%	4.16	3.73	9.14	1.52	0.035
	100%	4.62	4.26	5.57	1.55	0.033
H45	0%	4.05	4.27	12.40	1.51	0.030
	51%	4.16	4.49	0.89	1.52	0.046
	100%	4.62	4.90	56.00	1.55	0.022
H81	0%	4.05	4.02	10.77	1.51	0.025
	51%	4.16	4.17	4.30	1.52	0.029
	100%	4.62	4.63	3.36	1.55	0.029

Table 6

Table 6. Fitted $\dot{\delta}$ values under dynamic out-of-plane compression

η	$\dot{\varepsilon}$	$\dot{\delta}$
51%	100	40±5
	10	8.5±0.5
	1	0.8±0.05*
	0.1	0.1±0.005
0%	100	8±5
	10	4.5±0.5
	1	0.8±0.05×
	0.1	0.1±0.005

*Singular point for H45, 0.95

×Singular point for H45, 0.65

Figure 14

Click here to download high resolution image

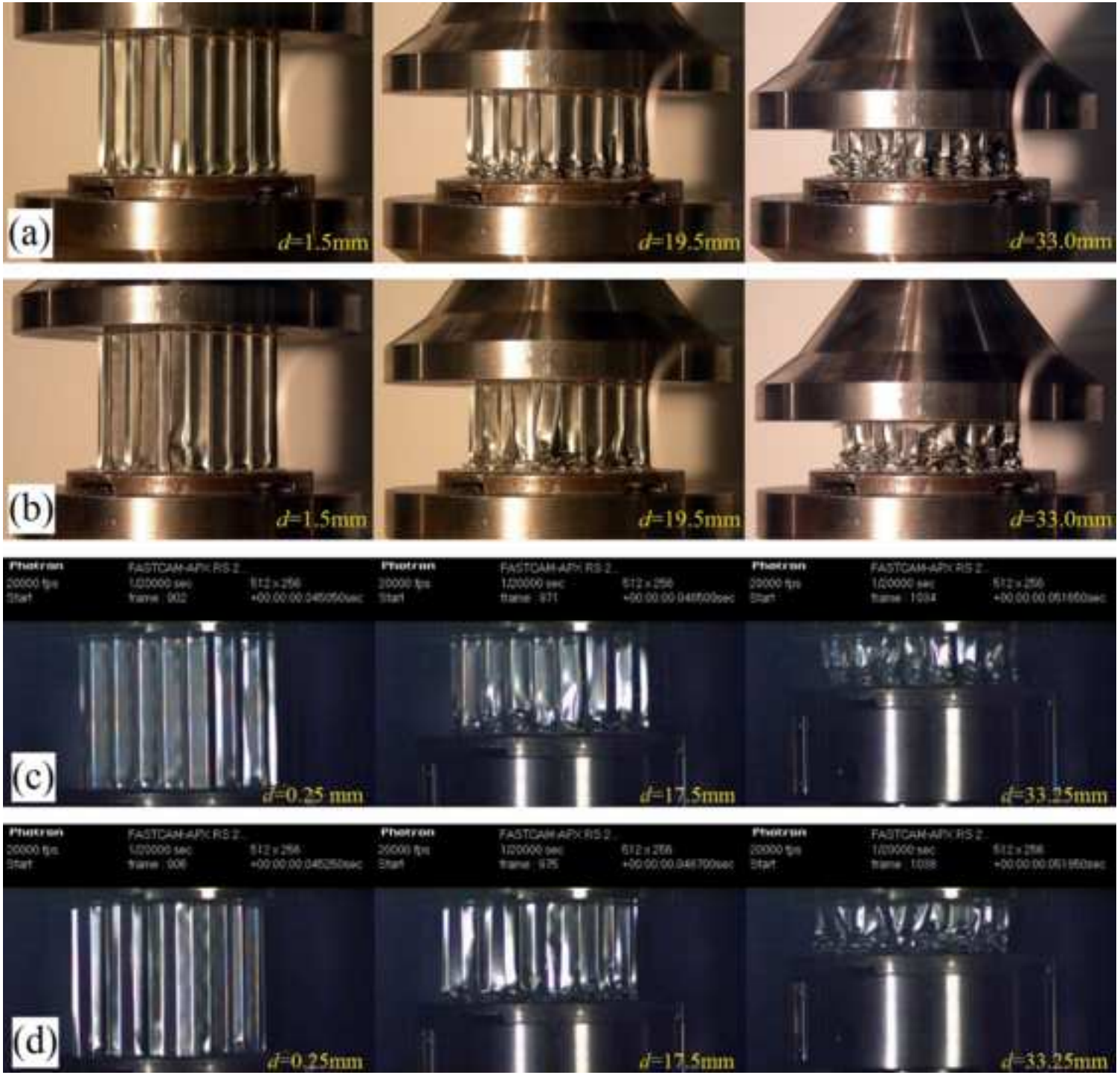

Figure Captions

Fig. 1. Procedure to make specimens: (a) a 4.2-3/8-5052-.003N specimen containing 5×5 cells covered by one layer of EP-280 films on each side; (b) one EP-280 film was penetrated by sharp ended heated tool; (c) the specimen covered by one layer of double sided glues on each side; (d) glue penetrated by heated tool; and (e) a typical 3.1-3/16-5052-.001N specimen containing 9×9 cells with 51% holes at one end.

Fig. 2. A sketch of the test set-up and the bottom support plate.

Fig. 3. Instron 8800 high rate testing system.

Fig. 4. Nominal stress-strain curves for honeycomb 3.1-3/16-5052-.001N under different compression velocities ranging from 5×10^{-5} to 5 m/s with hole percentage of: (a) 0%; (b) 51%; and (c) 100%.

Fig. 5. Nominal stress-strain curves for honeycomb 4.5-1/8-5052-.001N under different compressive velocities ranging from 5×10^{-5} to 5 m/s with hole percentage of: (a) 0%; (b) 51%; and (c) 100%.

Fig. 6. Nominal stress-strain curves for honeycomb 8.1-1/8-5052-.002N under different compression velocities ranging from 5×10^{-5} to 5 m/s with hole percentage of: (a) 0%; (b) 51%; and (c) 100%.

Fig. 7. Relationship between the mean plateau stress and t/l ratio under quasi-static compression.

Fig. 8. Relationship between the mean plateau stress and the strain rate for honeycombs: (a) 3.1-3/16-5052-.001N; (b) 4.5-1/8-5052-.001N; and (c) 8.1-1/8-5052.002N.

Fig. 9. (a) An example showing how to determine $\dot{\delta}$ and (b) dependence of $\dot{\delta}$ on the strain rate and the percentage of holes.

Fig. 10. Air pressure against the strain under different strain rates for specimens: (a) without holes; and (b) with 51% holes.

Fig. 11. Sketch of three types of stress-strain curves for honeycombs under out-of-plane compression.

Fig. 12. Comparison between the experimental dynamic compressive tests and the prediction (solid lines) of the plateau region without holes from quasi-static compression tests for honeycomb: (a) 3.1-3/16-5052-.001N; (b) 4.5-1/8-5052-.001N; and (c) 8.1-1/8-5052-.002N.

Fig. 13. Nominal stress-strain curves for honeycomb 4.2-3/8-5052-.003N under different compression velocities ranging from 5×10^{-5} to 5 m/s with hole percentage of: (a) 0%; (b) 51% and (c) 100%.

Fig. 14. Typical deformation pattern of under quasi-static and dynamic compression for honeycomb 4.2-3/8-5052-.003N with: (a) $\dot{\varepsilon}=10^{-3}$ s^{-1}, η=0%; (b) $\dot{\varepsilon}=10^{-3}$ s^{-1}, η=100%; (c) $\dot{\varepsilon}=10^{2}$ s^{-1}, η=0% ; and (d) $\dot{\varepsilon}=10^{2}$ s^{-1}, η=100%.